

Review

Benzodichalcogenophene-based Conjugated Polymers as Photovoltaic Materials

*Xin Lin Wong, Md Lutfor Rahman, Mohd Sani Sarjadi**

Faculty of Science and Natural Resources, University Malaysia Sabah, Jalan UMS, 88400 Kota Kinabalu, Sabah Malaysia

*E-mail: msani@ums.edu.my

Received: 5 April 2017 / Accepted: 17 May 2017 / Published: 12 June 2017

Conjugated polymers have appeared to be a promising electron-donating material in organic photovoltaics (OPVs). The designing of conjugated polymers is critical for improved efficiency and intensive efforts have devoted to design high-performance polymers over the past few decades. In this context, we focused on the use of heteroatom substitution in altering the physical properties of conjugated polymers. Owing to the increasing interest in the modification of thiophene-based conjugated polymers with Group 16 atoms, this work summarized the recent progress of these modifications and highlighted the impact of Group 16 atoms on the performance of conjugated polymers. Given polymers based on benzodithiophene (BDT) skeleton contributed largely to the recent progress of efficiency, we emphasized the subtle modification in benzodichalcogenophene-based polymers.

Keywords: Organic photovoltaic, conjugated polymers, chalcogens, benzodichalcogenophene

1. INTRODUCTION

1.1. Prologue

The development of photovoltaic devices has been advancing significantly for the past few decades with inorganic materials occupy the forefront of technology followed by the competence of organic materials. Despite having lower efficiency and lifetime than those of inorganic counterparts, organic photovoltaics (OPVs) are highly attractive owing to their lightweight, low-cost, ease of processing, and mechanical flexibility [1-7].

In recent years, the efficiency of polymer-based organic solar cells have improved rapidly from a power conversion efficiency (PCE) of below 1% in the 1990s to more than 10% recently [8-13],

showing their potential to be commercialized. This encouraging progress is mainly achieved by the molecular engineering of the structure of semiconducting conjugated polymers which act as active components in bulk-heterojunction (BHJ) photovoltaic device. The typical device configuration is shown in Figure 1.

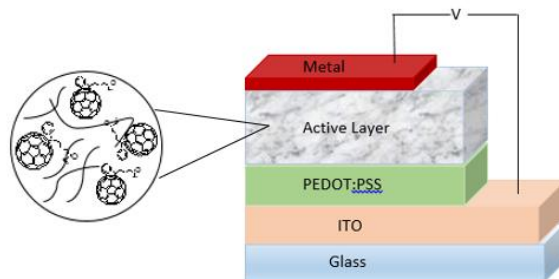


Figure 1. Architecture of a typical bulk heterojunction photovoltaic device.

The molecular design and synthesis of conjugated polymers is challenging as it involves a lot of criterion to be take care of during the process. In order to obtain a high PCE polymeric solar cell, conjugated polymers should have broad and strong optical absorption in the solar spectral range so that the short-circuit current (J_{sc}) is high; matched energy levels with those of acceptor materials for efficient exciton dissociation; high charge carrier mobility to facilitate exciton separation and diffusion; and good solubility in organic solvents for solution processing [14-16].

Donor-acceptor (D-A) structure is currently the most effective system used in achieving the requirements mentioned above. This strategy involves the copolymerization of electron-rich donor moieties (D) and electron-deficient acceptor moieties (A) alternatively which induces intramolecular charge transfer (ICT) between D and A units, leading to a narrowing of optical bandgap as depicted in Figure 2.

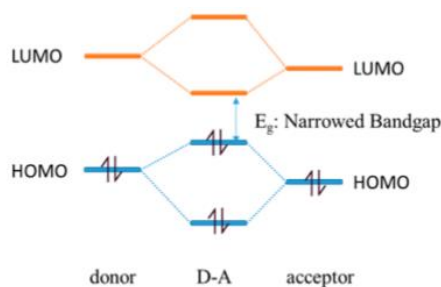


Figure 2. Molecular orbital hybridization of the D-A copolymer. Reprinted with permission from Yao, H., Ye, L., Zhang, H., Li, S., Zhang, S., and Hou, J. (2016) Molecular design of benzodithiophene-based organic photovoltaic materials, *Chemical Reviews*, 116, 7397-7457. Copyright (2016) American Chemical Society

In a D-A polymer system, the selection of donor and acceptor units is of paramount important as it governs the energy levels and the bandgap of a conjugated polymer. The magnitude of bandgap

affects the electronic and optical properties of conjugated polymers significantly. Nevertheless, substituents can be used to further fine tune the physical properties of conjugated polymer which will bring an adverse effect to the overall performance of the conjugated polymer.

For conjugated polymers containing heterocycles, the heteroatoms can be changed to further modify their properties. Among the five-membered heterocyclic compounds, thiophene, a sulphur-containing heterocycle, is one of the most widely used building blocks in the synthesis of conjugated polymer owing to its high synthetic versatility, π -conjugated character, and commercial availability. Nevertheless, interest in the chemistry and use of other Group 16 elements in organic photovoltaic has arisen for the past few years as can be seen from the surge in the number of papers published.

In this context, the properties and photovoltaic performance of analogues conjugated polymers containing Group 16 elements will be discussed, mostly based on the recent studies. By using the structural advantage of BDT unit [17], we highlighted the impact of heteroatom substitution on benzodichalcogenophene-based polymers. This review will focus on the correlation between chemical structure, physical properties and resulting device performance of the polymers, so as to promote further understanding to the influence of Group 16 elements on the performance of materials.

1.2. Characterization of Solar Cells

The performance of a solar cell is governed by a series of factors. Among these factors, the properties of the active layer's material possess the greatest influence on the overall performance of polymer solar cells [18]. The candidacy of a polymer as donor material in the active layer of the solar cell is largely determined by the power conversion efficiency (PCE) of a device. This device's efficiency relies on parameters open-circuit voltage (V_{OC}), short-circuit current (J_{SC}), and fill factor (FF) of the device as showed in equation (1). P_{in} is the incident light power which is standardized as 100 mW/cm^2 .

$$PCE (\eta) = \frac{J_{SC} V_{OC} FF}{P_{in}} \quad (1)$$

V_{OC} is the voltage measured across the device when current flow is zero [19]. It is strongly related to the energy level difference between the highest occupied molecular orbital (HOMO) level of the polymer donor and the lowest unoccupied molecular orbital (LUMO) level of the acceptor material. Although polymers with low-lying HOMO levels are theoretically more favourable to get high V_{OC} , the HOMO level of donor polymer cannot go too low. This is because the energy difference between the LUMO of donor and the LUMO of acceptor should be more than 0.3 eV for efficient exciton splitting and charge dissociation [9,15].

The number of excitons created upon light absorption decides the maximum value of J_{SC} for any excitonic solar cell [9]. J_{SC} is the current produced when there is no load across the device. It improves with the electron-donating ability of the polymer. The transport efficiency of electron and hole in the active layer also affect the J_{SC} value. The actual J_{SC} of a polymer solar cell is usually lower than the theoretical J_{SC} as charge recombination occurs easily during charge generation, transport, and extraction which lead to the loss of charges and thus the reduction of generated photocurrent [9].

FF is a measure of the rectification of the device. It is given by the ratio of actual maximum power output of solar cell to its theoretical power output (Equation 2) [20].

$$FF = \frac{J_m \times V_m}{J_{sc} \times V_{oc}} \quad (2)$$

In theory, the maximum value of FF is 1.0. However, it is hard to achieve FF above 0.83 in practice [20]. The FF of many polymer solar cells reported to date is typically in the range of 0.5-0.7. This mediocrity of performance is primarily due to the sensitivity of FF to the bulk properties of the photoactive layer and the interfacial properties between each layer [21, 22]. As explained in the work of Kim et al., the characteristic properties of the organic layer like morphology and thickness, the regioregularity of conjugated polymer, and the two interfaces between the electrodes and the blend layer affect the FF significantly through their influences on the series resistance (R_s) and the shunt resistance (R_{sh}) [23].

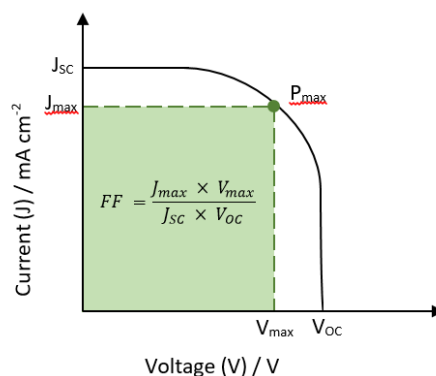


Figure 3. Current-voltage curves of an organic solar cell.

1.3. The Chemistry of Group 16 Heterocycle

Group 16 contains the elements oxygen (O), sulphur (S), selenium (Se), tellurium (Te), polonium (Po), and the synthetic element livermorium (Lv). The first four elements are often referred to as the chalcogens. They have been incorporated into five-membered heterocycles successfully as shown in Figure 4. Although these elements resemble one another in their chemical behaviour owing to similar valence electron configuration, their physical properties vary considerably which give different impact on their substitution in heterocycles.

Like the trends in other groups, the atomic radius of chalcogens increase down the group ($O < S < Se < Te$). This increased in size of the heteroatom will lengthen the $X-C\alpha$ bond of heterocycle and decrease the $C\alpha'-X-C\alpha$ heteroatom bonding angle [24]. Selenium and tellurium, thus, encounter relatively large steric effect when couple with other heterocycles as compared with the small size oxygen. The inherent small atomic radius of oxygen facilitates the planarity between neighbouring heterocycles. For selenium- and tellurium-containing copolymers, planarity can be improved through

their strong intermolecular interaction between neighbouring atoms which arise from the larger more polarizable radius of heteroatom.

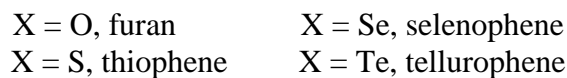
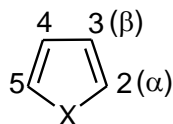


Figure 4. Structure of the five-membered heterocycles

Besides, this geometry alteration reveals the poor orbital overlap in larger chalcogenophenes, between the heteroatom and the π -system located on the carbon atoms [25, 26]. As a result, the double-bond character increases and the inter-ring C-C bond lengths decreases, indicating a loss of aromaticity in larger chalcogen heterocycles [25, 26].

The aromaticity of cyclic conjugated systems is typically evaluated by comparing the resonance energy. Resonance energy is also known as delocalization energy, which associates with compounds that have delocalized electrons. Delocalized electrons give extra stability to a ring system. The incorporation of electrons into the heterocycles' π -system is affected by the electronegativity of the chalcogens. Since sulfur has the lower electronegativity (2.56) as compare with oxygen (3.44), the electron pair on sulfur is more effectively incorporated into the conjugated system, that is, its delocalization produces more energy [27].

The resonance energy of heterocyclic compounds can be determined either experimentally through the use of empirical resonance energy (ERE) or theoretically with the Dewar resonance energy (DRE) model. For thiophene, its ERE value is ca. 120 kJ mol⁻¹ and its DRE is quoted as 27.2 kJ mol⁻¹. The ERE and DRE values found for furan are 80 kJ mol⁻¹ and 18 kJ mol⁻¹ respectively [28]. These values have confirmed the less aromaticity of furan than that of thiophene. The resonance energies for thiophene, however, are less than benzene (150.2 kJ mol⁻¹ for ERE and 94.6 kJ mol⁻¹ for DRE). Therefore, the order of aromaticity is benzene > thiophene > selenophene > tellurophene > furan [24].

Apart from aromaticity, dipole moments of chalcogenophenes are also influenced by the electronegativity of heteroatoms. A low electronegativity favours the incorporation of electrons into the conjugated system. The electrons on sulfur, selenium, and tellurium thus, are more readily delocalised towards the heterocycles rings than those on oxygen are, considering the electronegativity of heteroatom decreases as going down the group. This gives furan the largest reported dipole moment and tellurophene the smallest. Carbon-oxygen bonds are polarized $O^{\delta-}-C^{\delta+}$ while the low electronegativity of tellurium causes the carbon-tellurium bonds to be polarized inversely as $Te^{\delta+}-C^{\delta-}$.¹ As we know dipole moment is a measure of the polarity of a molecule, the larger difference in dipole moment of furan is likely the reason furan-based polymers exhibit better solubility in polar solvents than the other chalcogenophenes.

Numerous methods have been reviewed previously for the preparation of furan [29], thiophene [30], and their derivatives. Reviews on the synthesis and properties of selenophene [31], tellurophene,

and their derivatives are comparatively low. Nevertheless, there is an increase in the number of methods for their preparations over the past two decades which positively affect their uses in conjugated polymers.

All of these electron-rich, five-membered heterocycles undergo electrophilic substitution reactions with great ease as compare with benzene. For instance, furan undergoes electrophilic substitution about 10^{11} times faster than benzene under similar conditions. The relative reaction rates decrease in order of furan > tellurophene > selenophene > thiophene. Substitution usually occurs regioselectively at the α -positions unless these positions are occupied. Furan can also react by addition and/or ring-opening depends on the reagent and reaction conditions. For thiophene, further reactions like oxidation and desulfurization might take place due to the presence of sulfur [28].

2. DONOR-ACCEPTOR COPOLYMERS OF BENZODICHALCOGENOPHENE

2.1. Group 16 atoms in donor moieties

The earliest introduction of benzo[1,2-b:4,5-b']dithiophene (BDT) unit as photovoltaic material in PSCs was done by Hou and co-workers in 2008 [32]. Since then, a great number of BDT-based polymers were designed, synthesized, and applied in PSCs. Many of these BDT-based polymers are high performance polymers owing to the excellent intrinsic properties of BDT. BDT possess planar and symmetrical conjugated structure which facilitates the formation of π - π stacking, thereby enhance electron delocalization and improve charge mobility [32, 33]. Also, various substituents can be covalently connected on the 4 and 8 positions of BDT to optimize the solubility and energy levels of materials. A series of PSCs devices based on the blend of BDT-containing polymers and fullerene derivatives have showed promising PCEs of over 7% [34].

Replacing the sulfur atoms of BDT unit with oxygen atoms yields benzo[1,2-b:4,5-b']difuran (BDF) skeleton. Furan and its derivatives received much less attention in the field of organic semiconductors as compare with thiophene-based heteroaromatic units. The first application of BDF-based polymers in PSC was reported by Huo and co-workers in 2012 [35]. BDF was copolymerized with 4,7-dithienyl-2,1,3-benzothiadiazole (DTBT) and gave **P1** that showed a promising PCE of 5% when blended with PC₇₁BM in PSC. Device based on the sulfur analogue **P2** [36], however, only achieves a PCE of 1.95% despite having higher molecular weight than **P1**. The higher device efficiency for **P1** might be a result of better J_{SC} and FF. The HOMO level of **P1** has found to be lower than that of **P2** by 0.3 eV. Also, the optical bandgap of **P1** (1.60 eV) is significantly smaller than that of **P2** (1.85 eV). This is probably due to the smaller atomic size of oxygen atom which gives weaker steric hindrance to the adjacent unit, thereby forms a well planar configuration that facilitates the π -electrons delocalization along the conjugated backbone, leading to a smaller bandgap.

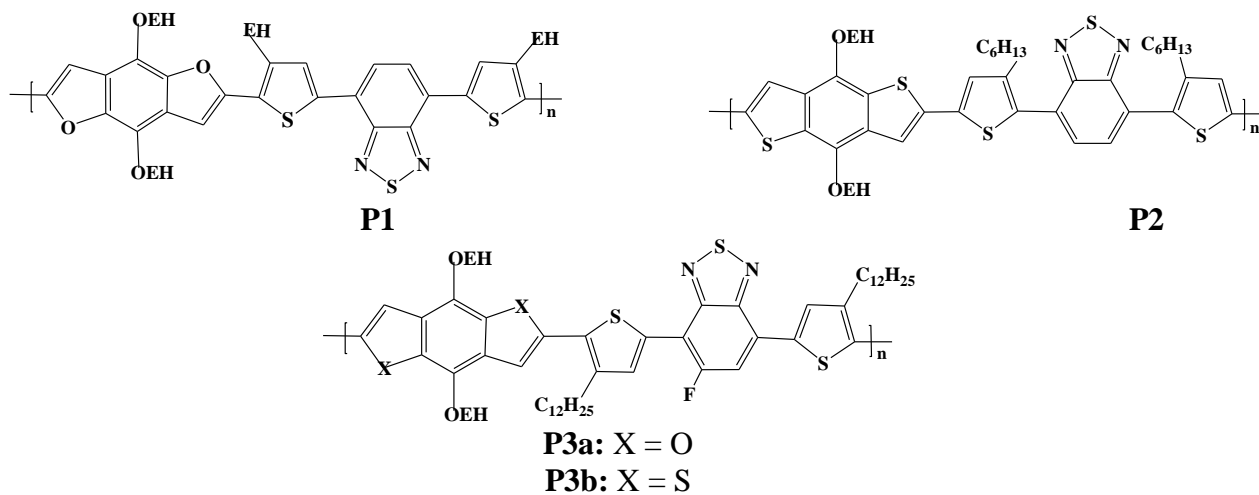
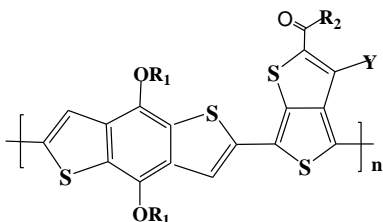


Figure 5. Chemical structures of benzodichalcogenophene-based copolymers.

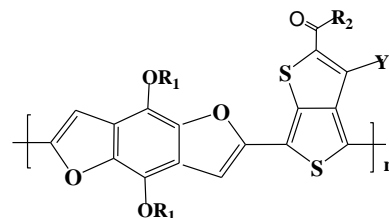
Similarly, polymer based on BDF and fluorinated benzothiadiazole (**P3a**) showed a lower optical band gap (1.60 eV) than its analogous BDT-based polymer **P3b** (1.64 eV) [37]. The introduction of fluorine atom has notably lowered the HOMO and LUMO energy levels of **P3a** and **P3b** as compared with that of the nonfluorinated analogues **P1** and **P2**. When blended with PC₇₁BM in 1:2 w/w, **P3b** showed a smoother blend film than that of **P3a** which indicated better miscibility of **P3b** with PCBM. This is likely the reason **P3b** exhibits a higher hole mobility (4.98×10^{-2} cm²/vs) than that of **P3a** (1.83×10^{-2} cm²/vs). Due to the higher mobility and better morphology, the PCE of **P3b**-based solar cell device reached 4.0%, which surpassed the 3.1% obtained from **P3a** device under the same conditions. It is noteworthy that this good performance of **P3b** is obtained without annealing or any additives.

The incorporation of thieno[3,4-b]thiophene (TT) unit in BDT-based polymers has led to numerous high performance polymers [38]. An impressive example of these PBDTTT-based polymers is **P4c**, which is synthesized by Liang and co-workers in 2010 through the conjugation of alkoxy-substituted benzodithiophene and fluorinated TT unit [18]. **P4c** has showed a high device efficiency of 7.4% in conventional PSCs. With the same conjugated backbone as the subject of study, He and colleagues (2012) has demonstrated that the efficiency of PSCs can be further enhanced to 9.2 % in an inverted device structure [39]. Compared to BDT, studies on copolymers with alternating BDF and TT units were lesser. In 2013, Liu and co-workers reported a BDF polymer structure with alkylcarbonyl-substituted TT acceptor (**P5a**) [40]. As expected, **P5a** has a smaller optical bandgap (1.48 eV) than that of its sulfur counterpart, **P4a** (1.60 eV) [41]. Replacing the sulfur atoms of BDT with the more electronegative oxygen atoms are lower the HOMO level of **P5a** significantly to -5.27 eV as compared with -5.07 eV of **P4a**. Although **P5a** has a deeper HOMO level, its V_{OC} is lower than that of **P4a**. This suggests that the V_{OC} of polymers can be affected by a couple of factors other than just the HOMO level of polymer. **P4a** showed a higher PCE of 6.43% compared to 4.4% of **P5a** when blended with PC₇₁BM in 1:1.5 w/w. This result can be assigned to the fact that **P4a** exhibits higher values for both V_{OC} and J_{SC} as compared with that of **P5a**. Also, an over 70% of maximum external quantum efficiency (EQE) value was achieved in **P4a** device at 490 nm, further explains its better photovoltaic

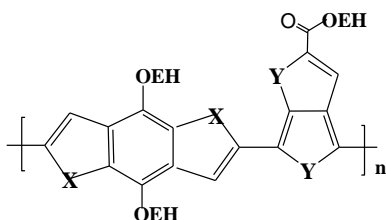
performance compared to the **P5a** device (with a maximum EQE value of 55% at 496nm). With an octyl side chain and a fluorine substituent, the analogue of **P4a**, **P4e** [42] has achieved a PCE as high as 7.73%. In 2013, a series of BDF-*alt*-TT copolymers (**P5c-e**) [43] has been reported by Huo and co-workers, with different electron-withdrawing groups attached to the TT units. These polymers showed decent photovoltaic performance with PCEs in a range of 4.26% - 5.23%, which is comparable to 5.10% of their sulfur analogue **P4d** [44].



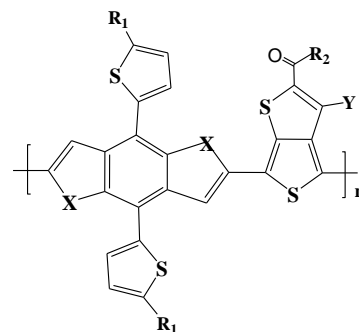
- P4a:** $R_1 = R_2 = \text{EH}$; $Y = \text{H}$
P4b: $R_1 = \text{EH}$; $R_2 = \text{OEH}$; $Y = \text{H}$
P4c: $R_1 = \text{EH}$; $R_2 = \text{OEH}$; $Y = \text{F}$
P4d: $R_1 = \text{C}_8\text{H}_{17}$; $R_2 = \text{OEH}$; $Y = \text{H}$
P4e: $R_1 = \text{EH}$; $R_2 = \text{C}_8\text{H}_{17}$; $Y = \text{F}$



- P5a:** $R_1 = R_2 = \text{EH}$; $Y = \text{H}$
P5b: $R_1 = R_2 = \text{EH}$; $Y = \text{F}$
P5c: $R_1 = \text{C}_8\text{H}_{17}$; $R_2 = \text{EH}$; $Y = \text{H}$
P5d: $R_1 = \text{C}_8\text{H}_{17}$; $R_2 = \text{OEH}$; $Y = \text{F}$
P5e: $R_1 = \text{C}_8\text{H}_{17}$; $R_2 = \text{EH}$; $Y = \text{F}$



- P6a:** $X = \text{Se}$, $Y = \text{S}$
P6b: $X = \text{Se}$; $Y = \text{Se}$
P6c: $X = \text{S}$; $Y = \text{Se}$



- P7a:** $R_1 = R_2 = \text{EH}$; $X = \text{S}$; $Y = \text{H}$
P7b: $R_1 = \text{EH}$; $R_2 = \text{OEH}$; $X = \text{S}$; $Y = \text{F}$
P7c: $R_1 = R_2 = \text{EH}$; $X = \text{O}$; $Y = \text{F}$

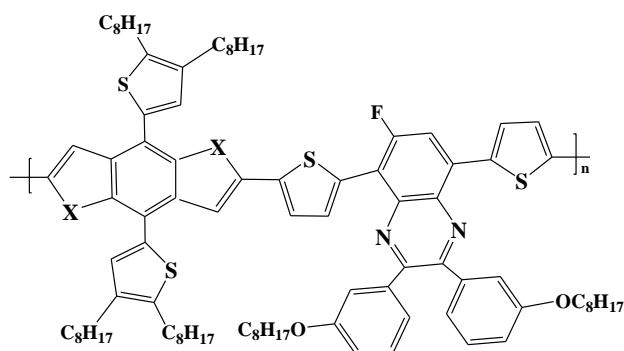
Figure 6. Chemical structures of benzodichalcogenophene polymers with thieno[3,4-b]thiophene electron acceptors.

The effect of selenium atom on the properties of polymers can be overviewed in the work of Luping Yu et al. (2012) who introduced selenium atom to replace the sulfur atom in BDT and TT units [45]. The replacement of sulfur by selenium in BDT unit yields **P6a**. A PSC device based on **P6a**/PC₇₁BM (1:1.5) shows a PCE of 6.13%, which is much higher than that of device based on its sulfur counterpart **P4b** (5.66%). This is presumably due to **P6a**'s ca. 36 nm red-shifted spectral covering and much greater V_{OC} value. The bathochromic shift of absorption spectrum becomes more significant as the selenium content in polymers increases. It can be noticed that **P6b** with selenium substituted in both BDT and TT units, showing an absorption maximum at 712 nm which is higher than 672 nm of **P4b**, 697 nm of **P6a**, and 702 nm of **P6c**. Also, **P6b** possess the highest hole mobility, $1.35 \times 10^{-3} \text{ cm}^2/\text{Vs}$, leading to a PCE of 6.87% as the best one among the four polymers. This can be

attributed to the fact that selenium atom is much larger and more polarizable than sulfur, thereby forming stronger Se-Se interactions than those of the sulfur which improves the conductivity and charge mobility of polymer.

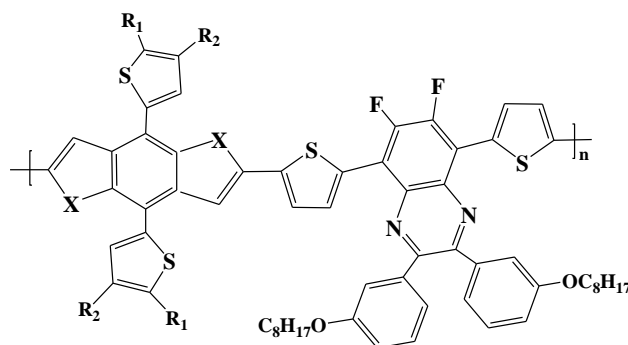
In recent years, 2-dimensional (2D) conjugated structure has received considerable attention owing to its potential to give high performance photovoltaic polymers. For instance, a PCE as high as 7.59% has been achieved with copolymer based on 2D BDT and TT units (**P7a**). The hole mobilities of **P7a** ($0.27 \text{ cm}^2/\text{Vs}$), determined by the space-charge-limited current (SCLC) model, is about 3 times higher than those of its non-conjugated counterparts **P4a** ($5.53 \times 10^{-4} \text{ cm}^2/\text{Vs}$) and **P5b** ($5.76 \times 10^{-2} \text{ cm}^2/\text{Vs}$). The relatively high charge carrier mobility can be rationalized by the fact that 2D conjugated polymers have higher planarity and much enhanced interchain π - π overlapping than those of their 1D counterparts. Considering the fascinating characteristics of a 2D conjugated structure, Liu and coworkers substituted the non-conjugated alkoxy side chains (in 1D **P4c**) with conjugated 5-alkylthiophene-2-yl side chains, forming 2D **P7b** [46]. The single-junction PSCs of **P7b** displayed a high J_{SC} of $19.6 \text{ mA}/\text{cm}^2$, V_{OC} of 0.79 V, and FF of 0.65, rendering an outstanding PCE of 10.12%. A photovoltaic device based on its oxygen analogue, **P7c** has also been reported with a PCE of 6.26%. The optical band gap of **P7c** (1.49 eV) is slightly lower than that of **P7b** (1.59 eV).

With two electron withdrawing imine nitrogen atoms, quinoxaline (Qx) and its derivatives have been widely used as strong acceptors to construct D-A copolymers. In 2015, Cong et al. reported two alternating polymers (**P8a** and **P9a**) based on 2D conjugated BDF and fluorinated quinoxaline derivatives [47]. Compared to its sulfur counterpart **P8b** [48], both HOMO and LUMO levels of **P8a** are significantly lower. As a result, **P8a** has a smaller bandgap (1.67 eV) than that of **P8b** (1.72 eV). This can be explained by the fact that oxygen atoms are smaller in size than that of the sulfur, thereby reduce the distance of π - π stacking for charge carrier transport. Nevertheless, the J_{SC} of **P8a** is only half of **P8b** ($11.4 \text{ mA}/\text{cm}^2$), which could be a result of poor film's morphology that causes fast recombination of charges. Their differences in molecular weight impact the formation and morphology. A device based on **P8a**/PC₇₁BM (1:1) showed a V_{OC} of 0.83 V, a J_{SC} of $5.28 \text{ mA}/\text{cm}^2$, and FF of 0.51, giving a PCE of 2.22%. For **P8b**, a relatively high PCE of 7.61% was obtained, with a V_{OC} of 0.88 V, a J_{SC} of $11.4 \text{ mA}/\text{cm}^2$ and FF of 0.76. In comparison to the mono-fluorinated **P8a**, the double fluorinated polymer **P9a** showed a better performance in OPV with a PCE value of 4.44%. **P9b** and **P9c** [49] are the other two examples of double fluorinated quinoxaline-based copolymers.



P8a: X = O

P8b: X = S



P9a: X = O; R₁ = R₂ = C₈H₁₇

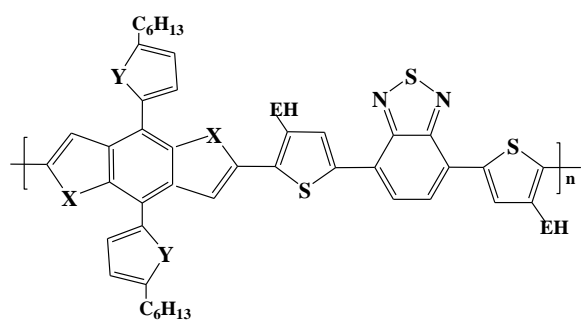
P9b: X = S; R₁ = C₈H₁₇; R₂ = H

P9c: X = S; R₁ = R₂ = C₆H₁₃

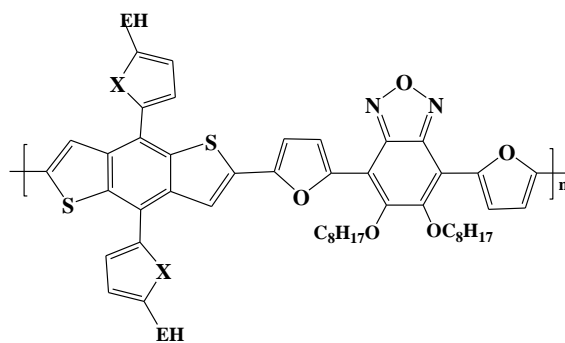
Figure 7. Chemical structures of benzodichalcogenophene polymers with fluorinated quinoxaline.

To investigate the effect of furan's substitution for thiophene, Zhang and co-workers (2013) designed and synthesized a series of 2D-conjugated copolymers based on BDT and BDF units with thiophene and furan units as the conjugated side-chains [50]. As compared with the all-sulfur-containing polymer **P10a**, furan-containing copolymers (**P10b**, **P10c**, and **P10d**) exhibited better OPV performance. Polymer **P10c** which composed of alternating alkylthienyl-BDF unit and benzothiadiazole unit gave the highest PCE value of 4.00% when blended with PC₇₁BM, with a V_{OC} of 0.79 V, a J_{SC} of 8.82 mA/cm² and FF of 57.4%. By adding 3% 1,8-diiodooctane (DIO) solvent additive, the device performance of **P10c** can be further improved to 4.42% which is over 2-fold higher than that of **P10a** (1.85%). The superior performance of **P10c** could be attributed to its higher hole mobility, 9.0×10^{-3} cm²/Vs. The replacement of sulfur atoms in BDT unit with the smaller atomic size oxygen is expected to give a more planar conjugated structure that is desirable for high charge mobility. The charge carrier mobilities can also be affected by the conjugated side chains. With furan conjugated side chain, polymer **P10b** possess an order higher of hole mobility, 6.1×10^{-4} cm²/Vs than that of its sulfur analogue **P10a** (2.5×10^{-5} cm²/Vs). This can be justified by the fact that the orbitals of oxygen atom overlap better with the π -system than the sulfur atom does, thereby gives the alkylfuranlyl group a stronger electron-donating ability. The HOMO levels of **P10b**, is higher than that of **P10a**. Also, the incorporation of alkylfuranlyl group down-shifted the LUMO levels of polymers as compared to those with the alkylthienyl group.

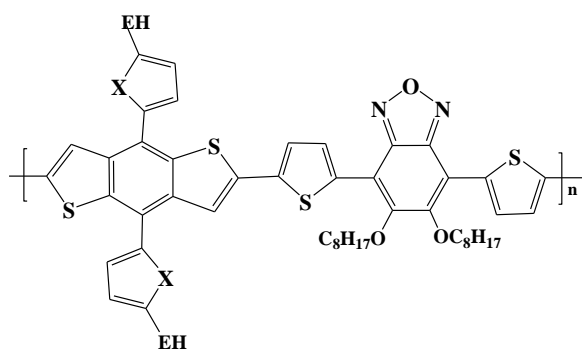
In 2013, Wang and co-workers synthesized 2D conjugated polymers **P11a** and **P11b** based on BDT and difuranylbenzoxadiazole moieties, with alkylfuranlyl and alkylthienyl as the conjugated side chains [51]. **P11a**, which has furan conjugated side chains, shows red-shifted absorption onset in both solution (672 nm) and thin film (700 nm) as compared with 661 nm and 686 nm of its sulfur counterpart **P11b**, indicating a broader absorption range for **P11a**. The optical bandgap deduced from the absorptions onset are 1.77 eV for **P11a** and 1.81 eV for **P11b**. Smaller bandgap coupled with broader absorption spectrum gives **P11a** a high J_{SC} of 12.8 mA/cm², FF of 0.62 and a high PCE of 6.6% which is surpass the 4.8% of **P11b**. The device performance for **P11a** and **P11b** can be boosted up to 7.0% and 5.0% respectively when the wetting time increased from 2 minutes to 3 minutes.



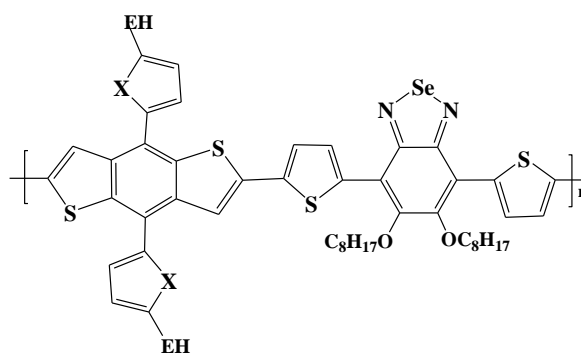
P10a: X = S; Y = S
P10b: X = S; Y = O
P10c: X = O; Y = S
P10d: X = O; Y = O



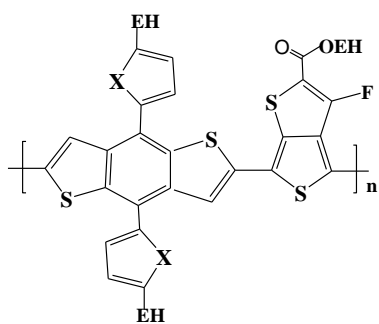
P11a: X = O
P11b: X = S



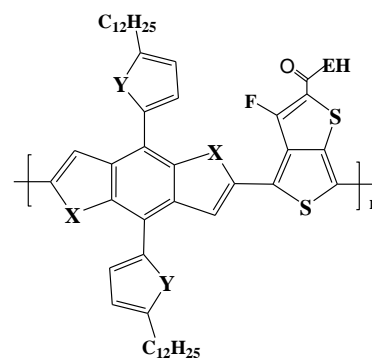
P12a: X = O
P12b: X = S



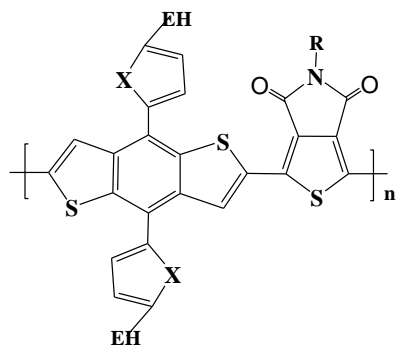
P13a: X = S
P13b: X = Se



P14a: X = O
P14b: X = S
P14c: X = Se



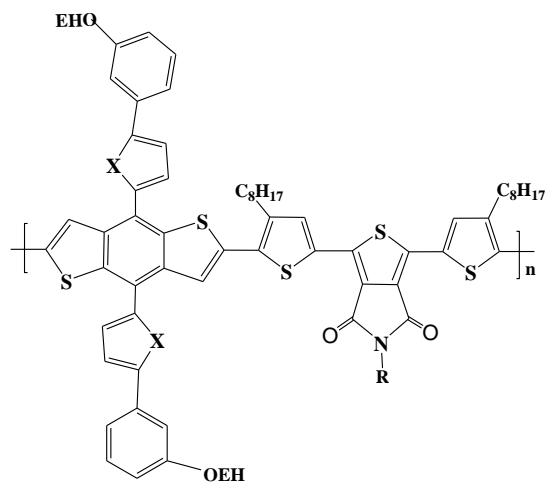
P15a: X = S; Y = S
P15b: X = S; Y = O
P15c: X = O; Y = S
P15d: X = O; Y = O



P16a: X = O; R = C₈H₁₇

P16b: X = S; R = C₈H₁₇

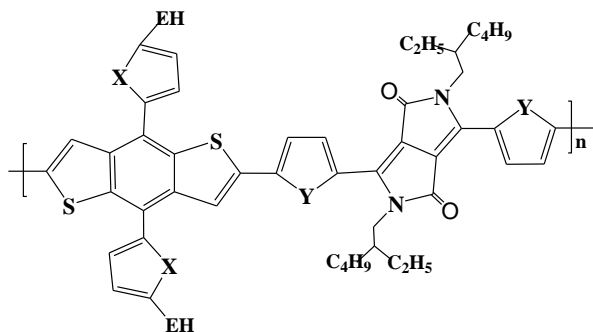
P16c: X = Se; R = C₈H₁₇



P17a: X = O; R = EH

P17b: X = S; R = EH

P17c: X = Se; R = EH

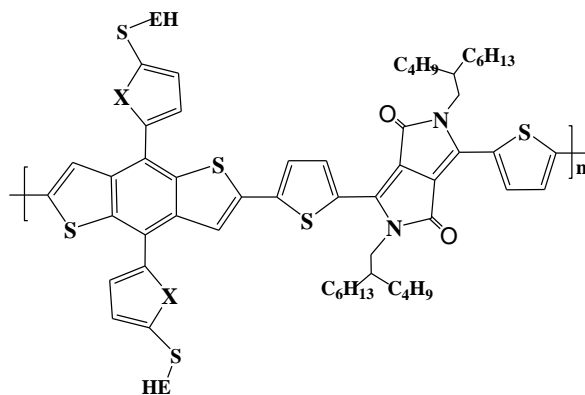


P18a: X = S; Y = S

P18b: X = O; Y = S

P18c: X = S; Y = O

P18d: X = O; Y = O



P19a: X = S

P19b: X = Se

Figure 8. Chemical structures of benzodichalcogenophene-based copolymers with various conjugated side chains

In the following year, two structurally similar copolymers **P12a** and **P12b** were reported by Jiang and co-workers (2014) [52]. As expected, **P12a** with furan conjugated side chain exhibited higher HOMO energy level (-5.38 eV) than that of its sulfur counterpart **P12b** (-5.46 eV). When blended with PC₇₁BM in the BHJ solar cell device, **P12b** achieved a high PCE value of 7.4% which outperformed the **P12a**/ PC₇₁BM-based device with a PCE of 5.4%. The better photovoltaic performance of **P12b** is likely due to its superior film's morphology which increases the charge carrier mobility in the active layer. The hole mobility of **P12b** (3.7×10^{-2} cm²/Vs) has found to be an order higher than 9.1×10^{-3} cm²/Vs of **P12a**.

In another study, Jiang's group (2014) grafted thiophene and selenophene side chains on the backbone of poly(benzodithiophene-alt-dithienyl[2,1,3-benzoselenadiazole]) to investigate the effect of selenium substitution on photovoltaic performance of polymers [33]. Interestingly, similar energy levels and bandgap were observed for **P13a** and **P13b**. This is probably due to the small difference in electronegativity of sulfur and selenium which gives thiophene and selenophene similar electron donating ability. Also, the authors found that the replacement of thiophene side chains with selenophene units did not affect the absorption edge but did enhance the absorption coefficient. A maximum PCE of 4.00% was achieved in PSC device based on **P13b**/PC₇₁BM (1:2 w/w) blend, with a high J_{SC} of 11.4 mA/cm², a V_{OC} of 0.67 V and FF of 52%. The device efficiency of **P13b** is better than that of a cell based on **P13a** (PCE = 3.30%) under the same conditions.

In 2014, Zhang and colleagues introduced furan, thiophene, and selenophene side chains on the BDT units and synthesized three copolymers, **P14a-P14c**, with fluorinated TT units as the electron acceptor [53]. The furan-substituted **P14a** has a narrower optical bandgap and an expectantly higher lying HOMO level than those of **P14b** and **P14c**. The authors found that the electron donating effect of chalcogens declined as their dihedral angles increased. **P14a** with the smaller atomic size oxygen atoms, thus, exhibited smaller dihedral angles than its sulfur and selenophene analogous, showing a higher HOMO level (-5.19 eV) than **P14b** (-5.24 eV) and **P14c** (-5.29 eV). The smaller dihedral angle of furan side chain resulted in a more efficient conjugation of the side chain and backbone. As a result, the film of **P14a** gave a broad absorption spectrum with an absorption maximum at 720 nm. **P14b** and **P14c** films showed comparatively blue-shifted absorption maxima (700 nm and 699nm respectively), corresponding to optical bandgaps of 1.58 eV. Despite having broader absorbance and smaller bandgap, **P14a** performed poorer in every category (J_{SC} = 11.77 mA/cm², V_{OC} = 0.69 V, FF = 64.8%) when fabricated into OPVs device than the other two polymers did, leading to a PCE of 5.28%. A device based on **P14b**/PC₇₁BM (1:1.5 w/w) achieved a remarkable PCE of 9.0%, with a high J_{SC} of 16.86 mA/cm², V_{OC} of 0.78 V, and FF of 68.2%. OPV of the selenium-containing **P14c** also experienced high J_{SC} of 16.57, V_{OC} of 0.81 V and FF of 65.6%, giving a high PCE of 8.78%.

Huang and co-workers (2015) further investigated the impact of heteroatoms substitution in the following year by synthesizing a series of copolymers (**P15a-P15d**) comprising BDT/BDF as donor, TT as acceptor, along with thiophene and furan as conjugated side chains [54]. When replaced the thiophene side chains with furan units, **P15b** showed higher HOMO level (-5.07 eV) and smaller optical bandgap (1.52 eV) than its sulfur counterpart **P15a** (-5.15 eV; 1.56 eV). **P15c** and **P15d**, which have furan units in the polymer backbone, exhibit lower optical bandgaps (1.51 eV and 1.50 eV respectively) than those of **P15a** and **P15b**, suggesting that the substitution effect is more pronounced when it happens at the conjugated backbone. The introduction of furan building blocks in conjugated backbone also enhances the solubility of resulted polymers, giving the BDF copolymers (**P15c** and **P15d**) higher molecular weight than the BDT copolymers (**P15a** and **P15b**). The molecular weight of polymer affects the molecular packing, carrier mobility, and blend morphology notably. Copolymer **P15d** which has the highest molecular weight exhibits the highest charge mobility (4.99×10^{-4} cm²/Vs) among the four polymers, leading to an impressive PCE of 5.23% when blended with PC₇₁BM (1:1.5 w/w). The performance of **P15d** surpassed the PCE of **P15a** (2.55%), **P15b** (2.61%), and **P15c** (3.34%) under the same conditions.

Thieno[3,4-c]pyrrole-4,6-dione (TPD) is a symmetric planar molecule comprising an alkyl-substituted imide fused on the thiophene unit. The imide renders the unit a relatively strong electron-withdrawing property. Warnan and co-workers (2014) incorporated TPD unit in BDT-based copolymers and synthesized three polymers (**P16a–P16C**) with furan, thiophene, and selenophene side chains [55]. The resulted copolymers (**P16a–P16C**) exhibited low HOMO energy levels ranged from -4.85 eV to -5.01 eV, giving these polymers high V_{OC} (0.90 V – 1.0 V). The furan-substituted **P16a** had smaller optical bandgap (1.78 eV) than those of **P16b** (1.88 eV) and **P16c** (1.85 eV). Also, **P16a** displayed a red-shifted absorption onset compared to **P16b** and **P16c**. Nevertheless, the photovoltaic performance of **P16a** is the worst among the three polymers, with a J_{SC} of 7.8 mA/cm², V_{OC} of 0.90 V, FF of 0.42, and a PCE value of 3.0% after optimized with 3% processing additive DIO. A device based on a blend of **P16b**/PC₇₁BM (1:1 w/w) in the active layer gave a high J_{SC} of 11.1 mA/cm², V_{OC} of 1.0 V, FF of 0.58, and a high PCE of 6.5% under the same condition.

To study the effect of chalcogen on electron rich donor units, Chakravarthi and co-workers synthesized a new series of 2D π -conjugated polymers **P17a - P17c**, in which alkoxyphenyl-furan, alkoxyphenyl-thiophene, and alkoxyphenyl-selenophene substituted BDT as an electron rich donor unit and TPD as an electron deficient acceptor unit, respectively [56]. Among the three copolymers (**P17a–P17c**), the alkoxyphenyl-furan substituted **P17a** exhibited the lowest optical band gap (1.77 eV), which could be assigned to the low steric hindrance of furan in π -conjugated polymers as compared to thiophene and selenophene. The more twisted structures found in thiophene and selenophene side chain substituted **P17b** and **P17c** caused very little HOMO delocalization into the thiophene and selenophene rings than that of furan ring in **P17a**. Hence, a higher lying HOMO level is observed in **P17a** (-5.35 eV) as compared to -5.44 eV of **P17b** and -5.48 eV of **P17c**. The hole mobility of **P17a**, calculated using SCLC model, was 7.81×10^{-5} cm²/Vs which was an order smaller than those in **P17b** and **P17c** (3.10×10^{-4} and 1.13×10^{-4} cm²/Vs respectively). This can be attributed to the poor mixing and excess phase separation in **P17a**. As a result, solar cells made from **P17a**:PC₇₁BM only achieved a PCE of 1.54%.

In recent years, the diketopyrrolopyrrole (DPP) units have gained popularity in constructing photovoltaic polymers owing to their strong electron-deficient properties given by the amide groups. Polymer **P18a** [57], synthesized by the Stille copolymerization of DPP and alkylthienyl-substituted BDT units, possess a small optical bandgap of 1.35 eV and a low lying HOMO level at -5.21 eV. Replacing the thiophene side chain with furan units upshifted the HOMO level of **P18b** to -5.16 eV. **P18b** [58] also exhibited a larger J_{SC} of 10.46 mA/cm² as compared with 9.80 mA/cm² of **P18a**. However, both **P18a** and **P18b** have almost similar V_{OC} . When blended with PC₇₁BM, **P18a** showed a slightly higher PCE (3.91%) than **P18b** (3.50%) despite a lower J_{SC} . A similar pattern of data can also be observed in OPVs using copolymers **P17c** and **P17d**. The furan-containing **P18d** gives a higher J_{SC} (12.64 mA/cm²) than that of **P18c** (12.55 mA/cm²) yet shows a poorer efficiency (5.10% Vs 5.54%) owing to its low FF.

Wang and co-workers (2016) introduced alkylthio substituent on the thiophene and selenophene conjugated side chains to study the impact of these side chains on the BDT-DPP copolymers [59]. Since the sulfur atom of alkylthio substituent has a π -acceptor capability, the HOMO levels of the resulted copolymers, **P19a** and **P19b**, are lower than other analogous based on BDT and

DPP units. Besides, the HOMO level of **P19a** (-5.41 eV) is noticeably lower than its selenium counterpart **P19b** (-5.29 eV). The authors found that the dihedral angle between the alkylthiothiophene conjugated side group and BDT unit (53°) is slightly smaller than that in BDTSe (55.77°), thus giving **P19a** a more planar conjugated structure that facilitates electron delocalization. The maximum absorption peak of **P19a** film was located at 770 nm with an absorption onset at 838 nm. In comparison with that of **P19a**, the film of **P19b** showed a slightly red-shifted absorption peak (772 nm) along with an absorption onset at 840 nm. This is probably due to the larger atomic size of selenium as well as its less electronegativity than that of the sulfur atom which facilitates the extension of absorption spectrum. While both **P19a** and **P19b** exhibited similar optical bandgap, the J_{SC} of **P19a** was higher than that of **P19b**. As a result, a **P19a**-based device had a higher PCE of 5.62% as compared to 5.01% of **P19b**-based device.

2.2. Group 16 atoms as spacer

Generally, π -bridges are small chromophores that inserted between donor and acceptor units to modulate the backbones of conjugated molecules. Varying the π -bridges affect the conformation of conjugated molecule chain, thereby cause a change in optical, electronic, and photovoltaic performances of resulted polymers. Jiang and co-workers (2014) synthesized copolymers **P20a** and **P20b** based on alkylthienyl-substituted BDT unit and benzoselenadiazole unit with thiophene and selenophene as spacer molecules [33]. Replacing the thiophene spacers with selenophene units has red-shifted the absorption onset 60 nm from 732 nm (**P20a**) to 792 nm (**P20b**). The corresponded optical bandgaps were 1.69 eV for **P20a** and 1.56 eV for **P20b**. The broadening of absorption and narrowing of bandgap could be a result of the stronger heteroatomic interaction of selenium atom than those of the sulfur which enhanced the interchain interactions between polymer chains thereby improved the intermolecular charge transfer. Nevertheless, the J_{SC} of **P20a** (10.1 mA/cm^2) was slightly higher than 9.5 mA/cm^2 of **P20b**, which gave **P20a** a higher PCE value of 3.30% as compared to 3.0% of **P20b**.

With an identical conjugated backbone but different side chains, Kranthiraja's group (2015) further studied the effect of thiophene and selenophene π -bridges on the photovoltaic properties of polymers [60]. The incorporation of selenophene spacer deepen the HOMO levels of resulted polymers (**P21b** and **P21d**) regardless of the different alkyl side chains. Compared to the thiophene bridged polymers (**P21a** and **P21c**), the selenophene counterparts (**P21b** and **P21d**) showed considerably red-shifted absorption onset. Optical bandgaps estimated from the absorption onset were 1.76 eV, 1.69 eV, 1.76 eV, and 1.63 eV for **P21a**, **P21b**, **P21c**, and **P21d** respectively. The reduction in bandgap could be explained by the relatively lower aromaticity of selenophene unit which enhanced the quinoid nature in the polymer backbone thereby lower the bandgap energy and broaden the absorption band. Interestingly, the hole mobility of thiophene-bridged **P21a** ($7.3 \times 10^{-3} \text{ cm}^2/\text{Vs}$) is slightly higher than that of the selenophene-bridged **P21b** ($5.5 \times 10^{-3} \text{ cm}^2/\text{Vs}$). This is presumably due to the non-covalent interactions between the sulfur atom of thiophene spacer and the oxygen atom of the dialkoxyl group on the BT unit which gives **P21a** a more planar structure that facilitates charges transport. Nonetheless, the J_{SC} and FF of **P21a** are smaller than those of **P21b**, indicating a more severe charge recombination

in P20a. With higher J_{SC} (12.28 mA/cm²), V_{OC} (0.70 V), FF (58.90%), the PCE obtained in a **P21b**-based device was 5.07%, surpassed the 4.16% of **P21a**-based device. Similarly, the photovoltaic performances of selenophene-bearing **P21d** are better than its sulfur analogue **P21c**, showing a high J_{SC} of 12.22 mA/cm², a V_{OC} of 0.73 V, and a FF of 59.35%, leading to a promising PCE of 5.34%.

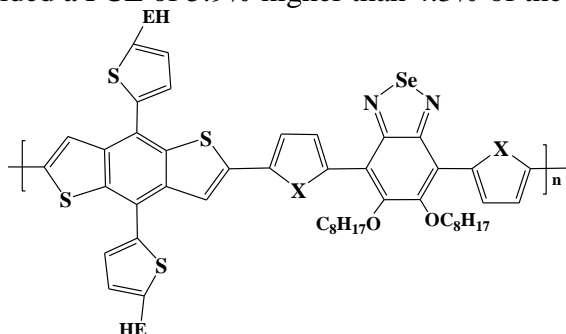
In 2012, Dou and co-workers evaluated the influences of chalcogen as π -bridges in the backbones of the PBDTT-DPP polymers [61]. When using selenophene as the π -bridge in the backbone of PBDTT-DPP, **P22c** showed a smaller optical bandgap and red-shifted absorption spectrum compared to its furan and thiophene counterparts. The authors attributed this phenomenon to the electron stabilizing effect of selenophene since selenium is more polarizable than either sulfur or oxygen. This intrinsic characteristic of selenium atom also offers selenium-containing units greater charge mobility owing to the strong interchain Se – Se interactions. The hole mobility determined by SCLC model were 2.2×10^{-4} cm²/Vs for **P22a**, 2.5×10^{-4} cm²/Vs for **P22b**, and 6.9×10^{-4} cm²/Vs for **P22c**. Due to the broader absorption coverage and higher EQE, **P22c** had higher J_{SC} value (16.8 mA/cm²) than those of **P22a** (10.9 mA/cm²) and **P22b** (13.7 mA/cm²). These results gave **P22c**/PC₇₁BM (1:2) based device the highest PCE (7.2%) among the three polymers despite low V_{OC} .

Being the structural isomer of DPP unit, pyrrolo[3,4-c]pyrrole-1,3-dione (DPPD), a pyrrole-based imide-functionalized electron-accepting unit, is expected to yield high performance photovoltaic polymers. In 2014, Tamilavan and co-workers incorporated thiophenes on both sides of DPPD unit and polymerized the resulting TDPPDT unit with electron-rich BDT unit to synthesized copolymer **P23a** [62]. **P23a** had a relatively large optical bandgap (2.11 eV) as the intrinsic electron-rich character of pyrrole in DPPD unit makes it a weak electron acceptor. The optical bandgap became smaller when replaced the thiophene spacers with selenophene units as depicted in **P23b** [63]. Also, the selenophene-containing **P23b** displayed slightly broader absorption band with 25 nm red-shifted absorption maximum compared with that of **P23a**. Nonetheless, the OPV performance of **P23a** was superior over that of **P23b**. A **P23a**-based device showed a high J_{SC} of 10.94 mA/cm², V_{OC} of 0.86 V, and FF of 71%, leading to a promising PCE have 6.74%.

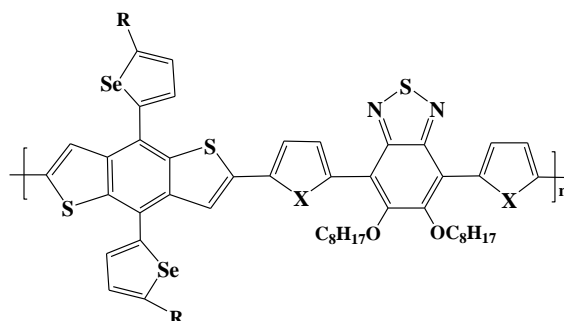
Tamilavan's group (2014) further optimized the structures of PBDT-DPPD polymers by introducing thiophene side chains on the BDT units to synthesize **P24a** and **P24b** [62, 63]. Compared to the alkoxy-substituted counterparts (**P23a** and **P23b**), copolymers with 2D side groups (**P24a** and **P24b**) showed better photovoltaic performance. Similar to the trend in **P23a** and **P23b**, **P24b** with selenophene π -bridges exhibited smaller bandgap and broader absorption spectrum than those of **P24a**. The substitution of thiophene π -bridges with selenophene units also downshifted both HOMO and LUMO levels of **P24b**. However, with a combination of high J_{SC} (10.12 mA/cm²), V_{OC} (0.90 V), and FF (72%), the device based on **P24a**/PC₇₁BM (1:2.5 w/w) obtained a higher PCE value (6.57%) than 4.45% of **P24b**.

Polymers **P25a** and **P25b** were prepared by Dang et al. (2014) based on alkylthienyl-substituted BDT moiety and fluorinated quinoxaline moiety with either furan or thiophene as conjugated spacers [14]. The furan-containing **P25a** showed a larger optical bandgap (1.87 eV) than that of **P25b** (1.77 eV), most probably due to the lower aromaticity of furan than that of thiophene. Besides, **P25a** displayed an obvious blue-shift absorption profile compare with that of its thiophene counterpart **P25b**. The absorption onset of **P25a** (667 nm) was 34 nm smaller than 701 nm of **P25b**.

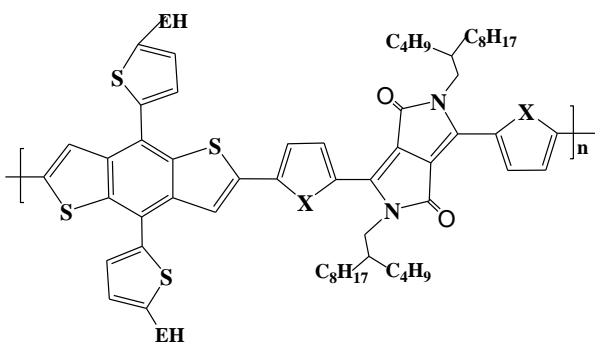
This blue-shift phenomenon could be a result of the relatively weak electron-donating properties of furan unit. Replacing the thiophene spacers with furan on both sides of the quinoxaline unit significantly lowered the HOMO level from -5.45 eV (**P25b**) to -5.71 eV (**P25a**), giving **P25a** V_{OC} as high as 0.91 V. Nevertheless, the J_{SC} of **P25b** (13.7 mA/cm²) was much greater than J_{SC} of **P25a** (9.1 mA/cm²), which could be explained by its higher hole mobility (1.0×10^{-4} cm²/Vs) as compared to that of **P25a** (9.0×10^{-5} cm²/Vs). When blended with PC₇₁BM (1:1 w/w), **P25b**-based PSC device yielded a PCE of 5.9% higher than 4.3% of the **P25a**-based device.



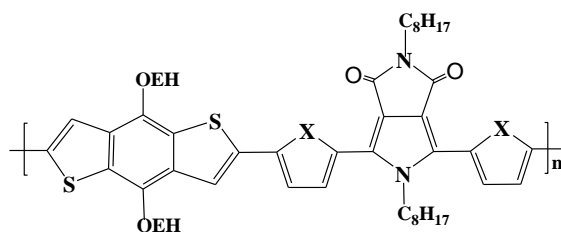
P20a: X = S
P20b: X = Se



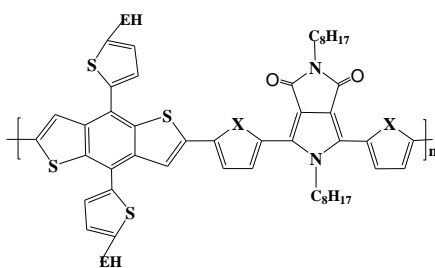
P21a: X = S; R = 2-ethylhexyl
P21b: X = Se; R = 2-ethylhexyl
P21c: X = S; R = 2-hexyldecyl
P21d: X = Se; R = 2-hexyldecyl



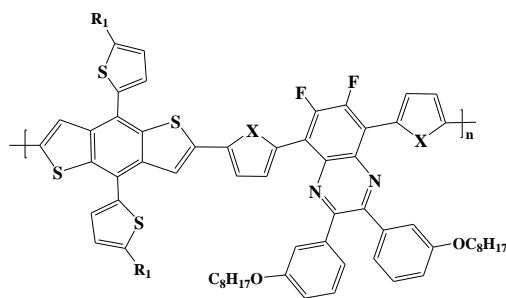
P22a: X = O
P22b: X = S



P23a: X = S
P23b: X = Se
P23c: X = Se



P24a: X = S
P24b: X = Se



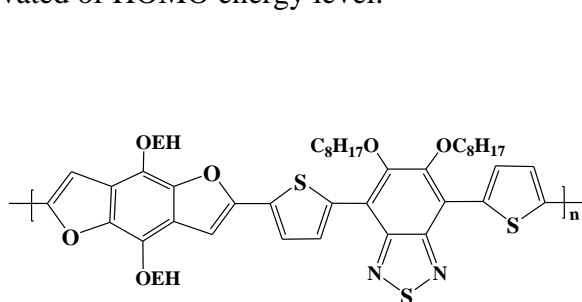
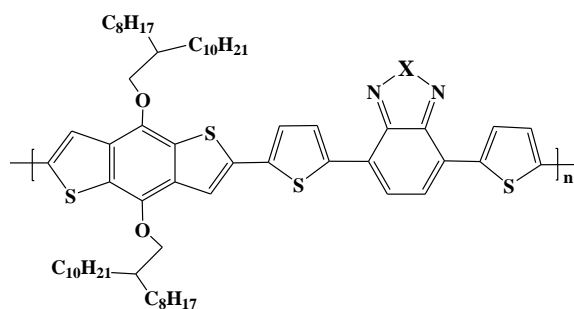
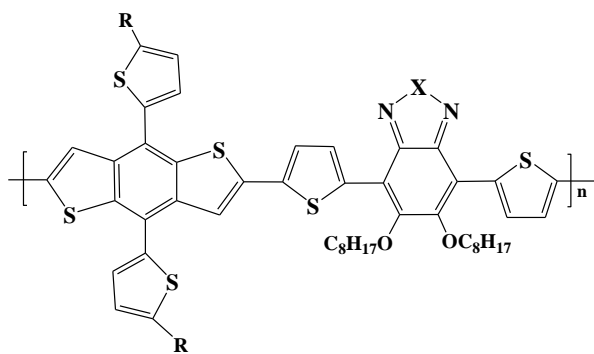
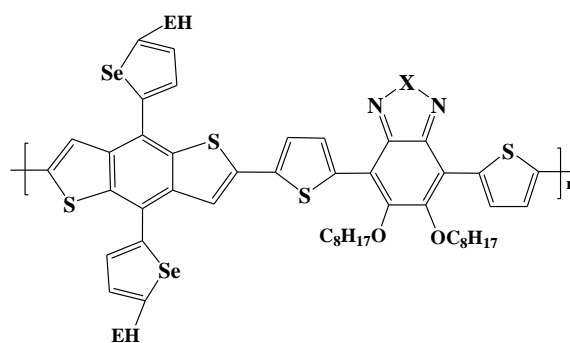
P25a: X = O
P25b: X = S

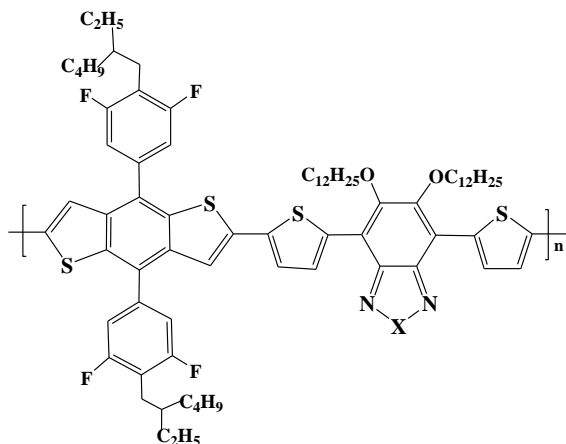
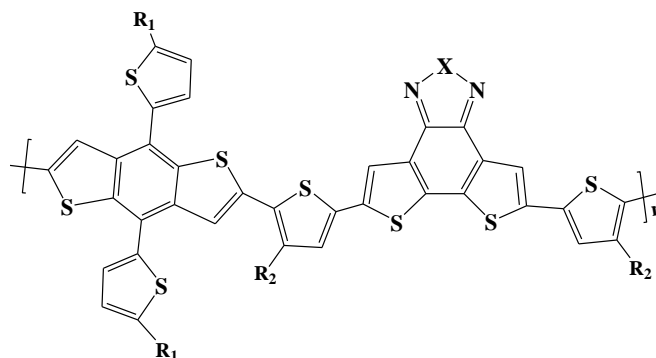
Figure 9. Chemical structures of BDT-based copolymers with different chalcogen spacers.

2.3. Group 16 atoms in acceptor moieties

Perhaps the most commonly employed acceptor unit in the benzodichalcogenophene based polymers is the 2,1,3-benzothiadiazole (BT) unit. Its strong electron-withdrawing nature coupled with commercial availability has attracted considerable research interest. Other Group 16 atoms like oxygen and selenium have been explored as the bridging atom to replace the sulfur atom in BT unit. In 2012, Liu and co-workers copolymerized an alkoxy-substituted BDF unit with the oxygen analogue of BT, benzoxadiazole (BO), giving polymer **P26a** [64]. Compared with the analogous BT polymer **P26b**, both HOMO and LUMO levels of **P26a** are lower, resulting in better air stability and higher V_{OC} . However, the hole mobility of **P26b** (6.72×10^{-2} cm²/Vs) was considerably higher than that of **P26a** (2.25×10^{-4} cm²/Vs). Hence, it is not surprising that the J_{SC} of **P26b** (9.87 mA/cm²) is nearly 50% higher than that of **P26a** (5.04 mA/cm²), yielding a PCE of 4.45% surpassing 2.88% of **P26a**-based device.

The selenium containing analogue to the BT unit is known as 2,1,3-benzoselenadiazole (BSe). To investigate the effect of selenium substitution, Zhou and co-workers (2013) synthesized copolymer **P27b** based on BSe unit and compared it with its sulfur counterpart **P27a** [65]. As compared with **P27a**, **P27b** showed a bathochromic shift in the absorption spectrum with absorption maximum red-shifted 34 nm from 646 nm (**P27a**) to 680 nm (**P27b**). The optical bandgaps estimated from the absorption onset were 1.72 eV for **P27a** and 1.55 eV for **P27b**. The broader absorption and smaller bandgap improved the hole transport of **P27b**, giving it a higher J_{SC} (13.58 mA/cm²) and FF (64%) than those of **P27a** ($J_{SC} = 11.16$ mA/cm²; FF = 62%). Hence, the PCE of a **P27b**-based PSC device (5.18%) was slightly higher than that of a **P27a**-based device (5.01%) despite lower V_{OC} owing to the elevated of HOMO energy level.

**P26a:** X = O**P26b:** X = S**P27a:** X = S**P27b:** X = Se**P28a:** X = O; R = 2-ethylhexyl**P29a:** X = S

P28b: X = S; R = 2-ethylhexyl**P28c:** X = Se; R = octyl**P29b:** X = Se**P30a:** X = O**P30b:** X = S**P31a:** X = O; R₁=2-butyloctyl; R₂=2-ethylhexyl**P31b:** X = S; R₁=2-butyloctyl; R₂=2-ethylhexyl**P31c:** X = Se; R₁=2-butyloctyl; R₂=2-ethylhexyl**Figure 10.** Chemical structures of Data of benzochalcogenodiazole-based copolymers.

Taking the advantages of 2D-BDT, Liu and colleagues (2013) continued their study via Stille coupling of alkylthienyl-substituted BDT unit with either BO or BT unit to synthesize **P28a** and **P28b** [66]. Interestingly, heteroatom substitution in this case shows more impact on HOMO levels than on LUMO levels. While both **P28a** and **P28b** have almost similar LUMO levels, the HOMO level of **P28a** experiences a drop of 0.10 eV. The deeper HOMO level of **P28a** resulted in a higher V_{OC} (0.84 V) than that of **P28b** (0.75 V). Also, **P28a** exhibited a larger J_{SC} (11.45 mA/cm²) than 10.29 mA/cm² of **P28b** due to its higher hole mobility. Thus, **P28a** demonstrated a high PCE of 5.90% when blended with PC₇₁BM in BHJ cell, outperformed 4.94% of **P28b**. In the following year, a 2D conjugated polymer (**P28c**) [67] based on selenium analogue of BT was reported by Shin et al. Replacing the sulfur atom of BT with selenium elevated the HOMO level of resulted polymer **P28c**, leading to a lower V_{OC} as compared with that of **P28b**. The overall photovoltaic performance of **P28c** was the poorest among the three polymers, with a V_{OC} of 0.67 V, J_{SC} of 10.23 mA/cm² and FF of 46%, yielding a PCE of 3.18%. Unfortunately, a direct comparison is misleading since **P28c** has different side chains with those of **P28a** and **P28b** which affects the morphology of film.

In addition to the copolymers discussed above, researches also designed several other benzochalcogenodiazole-based polymers by applying different donor units. For examples, Jiang and co-workers (2014) copolymerized alkylselenenyl-substituted BDT unit with thiophene-flanked BT and BSe to synthesize **P29a** and **P29b** respectively [33]. When replacing the sulfur atom in the electron-deficient moiety with selenium atom, the absorption onset red-shifted 35 nm and the optical bandgap became narrower. This is because selenophene has relatively lower aromaticity thereby enhances the ground-state quinoid resonance character of its resulting polymers, leading to improved planarity, lower bandgap energy, and broader absorption spectrum. Nevertheless, the HOMO level raised upon

selenium substitution which rendered **P29b** a lower V_{OC} . With better performance in every category ($V_{OC} = 0.86$ V, $J_{SC} = 13.9$ mA/cm², FF = 64%), BHJ device based on **P29a**:PC₇₁BM (1:2 w/w) achieved an impressive PCE of 7.6%, surpassing the 4.0% of **P29b**.

In 2016, Li and his fellow workers introduced 4-alkyl-3,5-difluorophenyl group on the BDT unit and synthesized **P30a** and **P30b** with either BO or BT as the acceptor unit [68]. Owing to the presence of oxygen, **P30a** has a more stabilize HOMO level (-5.62 eV) than the sulfur bearing **P30b** (-5.50 eV). This downshift of HOMO level gives **P30a** a higher V_{OC} (0.96 V) than that of **P30b** (0.89 V). The LUMO level also experienced a drop of 0.11 eV when substitution took place. Since the oxygen-containing **P30a** has a low-lying LUMO level at -3.80 eV, its LUMO offset is smaller than that of **P30b**, causing a negative effect on the charge separation. As a result, the hole mobility of **P30a** (2.3×10^{-5} cm²/Vs) is an order of magnitude smaller than that of **P30b** (1.3×10^{-4} cm²/Vs). Benefiting from the higher hole mobility, the BT-based polymer **P30b** exhibited higher J_{SC} (12.67 mA/cm²) which contributed to an inspiring PCE value of 8.24%. It is worth noting that no additive and postannealing treatments required for such a good performance. Conversely, 1% of DIO processing additive was needed for a **P30a**-based PSC device to produce a maximum PCE value of 5.67%.

Recently, Lee and co-workers reported a series of well-performing medium-bandgap conjugated polymers (**P31a-P31c**) based on fused dithienobenzochalcogenadiazole fDTBX moiety (X = O, S, and Se) [69]. The fDTBX unit is a modification of benzochalcogenophene unit, whereby the benzo function is fused with thiophene rings, restricting intramolecular rotation thereby maximize π -orbital overlap [70]. Owing to the electron-donating nature of the two fused thiophene rings, the electron-withdrawing property of the whole fDTBX moiety diminish. Thus, high lying LUMO energy levels were observed in **P31a-P31c**. The HOMO level values, as expected, increase on going from **P31a** (fDTBO) to **P31b** (fDTBS) to **P31c** (fDTBSe), corresponding to -5.51, -5.4, and -5.40 eV. The authors believe the gradual increase of HOMO level values is a result of destabilization in occupied bonding molecular orbital which arises from the decreasing ionization potential of heavier chalcogen atom. From the absorption spectra, more intense vibronic features were observed in both solution and thin film of **P31b** compared to those in **P31a** and **P31c**, suggesting the well-ordered intermolecular packing behaviours of **P31b** polymer chains. The more favourable morphology of **P31b**:PC₇₁BM thin film explained its highest photovoltaic performances (PCE = 5.34%) among the three polymers. When the molecular weight of **P31b** increased, the PCE of **P31b**-based device was found to improve from 5.34% to 6.02%, with a high J_{SC} of 10.80 mA/cm², V_{OC} of 0.84 V and FF of 0.66. This enhancement of performance was attributed to the improved crystalline ordering and BHJ morphological property of components in thin films.

Table 1. Data of benzodichalcogenophene-based copolymers

Polym er	M_n (kDa)	PDI	HOMO (eV)	LUMO (eV)	E_g^{opt} (eV)	V_{OC} (V)	J_{SC} (mA cm ⁻²)	FF	PCE (%)	Ref.
P1	6.3	1.6	-5.10	-3.24	1.60	0.78	11.77	0.55	5.01 ^b	[35]
P2	23.2	1.3	-4.80	-	1.85	0.84	6.28	0.37	1.95	[36]
P3a	5.4	1.2	-5.33	-3.58	1.60	0.62	9.17	0.58	3.30 ^b	[37]

P3b	6.1	2.5	-5.30	-3.57	1.64	0.72	9.31	0.60	4.00 ^b	[37]
P4a	21.0	3.7	-5.07	-3.21	1.60	0.70	15.51	0.59	6.43 ^b	[41]
P4b	35.6	2.1	-5.00	-3.13	-	0.60	14.3	0.66	5.66 ^b	[45]
P4c	46.4	2.1	-5.15	-3.31	-	0.74	14.50	0.69	7.40 ^b	[18]
P4d	16.8	1.4	-4.94	-3.22	1.59	0.60	12.8	0.66	5.10 ^a	[44]
P4e	-	-	-5.22	-3.45	1.60	0.76	15.2	0.67	7.73 ^b	[42]
P5a	21.0	2.1	-5.27	-3.69	1.48	0.66	10.45	0.64	4.40 ^b	[40]
P5b	4.7	3.0	-4.98	-3.18	1.51	0.63	13.87	0.60	5.22 ^b	[41]
P5c	40.7	1.7	-5.03	-3.63	1.53	0.54	13.13	0.60	4.26 ^b	[43]
P5d	61.0	1.7	-5.07	-3.61	1.53	0.61	15.75	0.54	5.17 ^b	[43]
P5e	45.3	2.4	-5.11	-3.60	1.52	0.63	13.88	0.60	5.23 ^b	[43]
P6a	28.2	1.9	-5.05	-3.27	-	0.64	14.6	0.66	6.13 ^b	[45]
P6b	15.2	2.7	-5.04	-3.26	-	0.64	16.8	0.64	6.87 ^b	[45]
P6c	9.1	1.7	-5.05	-3.27	-	0.60	15.4	0.59	5.47 ^b	[45]
P7a	20.0	3.2	-5.11	-3.25	1.58	0.74	17.48	0.59	7.59 ^b	[41]
P7b	45.0	2.4	-5.49	-3.74	1.59	0.79	19.60	0.65	10.12 ^b	[46]
P7c	4.7	3.6	-5.21	-3.20	1.49	0.78	13.04	0.62	6.26 ^b	[41]
P8a	24.9	2.73	-5.25	-3.20	1.67	0.83	5.28	0.51	2.22 ^b	[47]
P8b	76.0	3.29	-4.83	-2.22	1.72	0.88	11.40	0.76	7.61 ^b	[48]
P9a	75.7	2.69	-5.30	-3.25	1.68	0.83	8.74	0.61	4.44 ^b	[47]
P9b	25.0	2.56	-5.89	-3.61	1.70	0.84	11.10	0.61	5.70 ^a	[40]
P9c	30.0	2.20	-5.87	-3.63	1.77	0.96	6.50	0.54	3.40 ^a	[40]
P10a	6.8	4.8	-5.26	-3.34	1.67	0.88	5.83	0.36	1.85 ^a	[50]
P10b	7.6	3.0	-5.24	-3.54	1.70	0.85	8.41	0.40	2.88 ^a	[50]
P10c	4.0	2.9	-5.08	-3.39	1.68	0.73	9.94	0.61	4.42 ^a	[50]
P10d	5.2	2.5	-5.11	-3.60	1.61	0.80	5.84	0.56	2.60 ^a	[50]
P11a	38.4	2.2	-5.40	-3.61	1.77	0.84	12.8	0.62	6.60 ^a	[51]
P11b	29.3	2.0	-5.44	-3.59	1.81	0.87	9.4	0.59	4.80 ^a	[51]
P12a	60.6	4.7	-5.38	-3.44	1.78	0.81	11.2	0.60	5.40 ^a	[52]
P12b	62.5	4.3	-5.46	-3.47	1.78	0.86	12.8	0.67	7.40 ^a	[52]
P13a	45.1	3.5	-5.29	-3.60	1.69	0.66	10.1	0.50	3.30 ^a	[33]
P13b	47.2	3.4	-5.29	-3.60	1.69	0.67	11.4	0.52	4.00 ^a	[33]
P14a	5.7	1.9	-5.19	-3.64	1.55	0.69	11.77	0.65	5.28 ^a	[53]
P14b	22.0	2.0	-5.24	-3.66	1.58	0.78	16.86	0.68	9.00 ^a	[53]
P14c	69.0	2.3	-5.29	-3.71	1.58	0.81	16.57	0.66	8.78 ^a	[53]
P15a	23.0	3.2	-5.15	-3.36	1.56	0.73	6.30	0.54	2.55 ^a	[54]
P15b	33.6	2.6	-5.07	-3.29	1.52	0.67	6.63	0.59	2.61 ^a	[54]
P15c	50.6	4.1	-5.18	-3.53	1.51	0.68	8.09	0.60	3.34 ^a	[54]
P15d	66.7	5.1	-5.12	-3.56	1.50	0.65	12.33	0.64	5.23 ^a	[54]
P16a	14.5	2.4	-4.85	-2.76	1.78	0.90	7.80	0.42	3.00 ^a	[55]

P16b	16.4	3.1	-5.01	-2.76	1.88	1.00	11.10	0.58	6.50 ^a	[55]
P16c	12.7	3.2	-4.98	-2.76	1.85	0.98	8.70	0.48	4.70 ^a	[55]
P17a	11.0	2.2	-5.35	-3.58	1.77	0.80	5.29	0.36	1.54	[56]
P17b	17.9	2.2	-5.44	-3.59	1.85	0.92	8.90	0.41	3.37	[56]
P17c	19.5	2.0	-5.48	-3.67	1.81	0.96	7.84	0.47	3.53	[56]
P18a	80.0	3.6	-5.21	-3.60	1.35	0.68	9.80	0.59	3.91 ^a	[57]
P18b	26.4	5.4	-5.16	-3.64	1.44	0.69	10.46	0.49	3.50 ^a	[58]
P18c	57.2	2.5	-5.24	-3.55	1.41	0.73	12.55	0.60	5.54 ^a	[57]
P18d	30.5	5.6	-5.24	-3.74	1.47	0.72	12.64	0.57	5.10 ^a	[58]
P19a	65.5	2.5	-5.41	-3.60	1.48	0.79	13.18	0.54	5.62 ^a	[59]
P19b	46.1	3.2	-5.29	-3.60	1.48	0.76	11.34	0.58	5.01 ^a	[59]
P20a	45.1	3.5	-5.29	-3.60	1.69	0.66	10.10	0.50	3.30 ^a	[33]
P20b	38.7	3.1	-5.29	-3.73	1.56	0.67	9.50	0.49	3.00 ^a	[33]
P21a	59.0	1.86	-5.20	-3.44	1.76	0.69	11.75	0.53	4.16 ^a	[60]
P21b	46.0	1.78	-5.26	-3.57	1.69	0.70	12.28	0.59	5.07 ^a	[60]
P21c	51.0	1.80	-5.22	-3.46	1.76	0.71	10.38	0.58	4.30 ^a	[60]
P21d	45.0	1.76	-5.40	-3.77	1.63	0.73	12.22	0.59	5.34 ^a	[60]
P22a	35.2	2.1	-5.26	-3.64	1.51	0.77	10.90	0.56	4.70 ^a	[61]
P22b	40.7	2.1	-5.30	-3.63	1.46	0.73	13.70	0.65	6.50 ^a	[61]
P22c	38.4	2.1	-5.25	-3.70	1.38	0.69	16.80	0.62	7.20 ^a	[61]
P23a	13.6	1.6	-5.39	-3.28	2.11	0.86	10.94	0.71	6.74 ^a	[62]
P23b	10.9	1.9	-5.43	-3.43	2.03	0.74	7.42	0.39	2.26 ^a	[63]
P24a	18.5	2.0	-5.44	-3.40	2.04	0.90	10.12	0.72	6.57 ^a	[62]
P24b	11.0	2.2	-5.49	-3.53	1.97	0.79	10.85	0.52	4.45 ^a	[63]
P25a	35.0	3.1	-5.71	-3.45	1.87	0.91	9.10	0.53	4.30 ^a	[14]
P25b	58.0	2.0	-5.45	-3.56	1.77	0.77	13.70	0.56	5.90 ^a	[14]
P26a	27.0	1.2	-5.19	-3.49	1.70	0.82	5.04	0.70	2.88 ^a	[64]
P26b	7.0	2.0	-5.11	-3.38	1.73	0.69	9.87	0.65	4.45 ^a	[64]
P27a	22.0	2.1	-5.26	-3.50	1.72	0.72	11.16	0.62	5.01 ^a	[65]
P27b	20.1	2.1	-5.18	-3.48	1.55	0.60	13.58	0.64	5.18 ^a	[65]
P28a	41.3	1.7	-5.25	-3.28	1.69	0.84	11.45	0.61	5.90 ^a	[66]
P28b	16.7	1.5	-5.15	-3.30	1.66	0.75	10.29	0.64	4.94 ^a	[66]
P28c	11.0	4.3	-5.10	-3.45	1.67	0.67	10.23	0.46	3.18 ^a	[67]
P29a	67.3	4.1	-5.46	-3.68	1.78	0.86	13.90	0.64	7.60 ^a	[33]
P29b	47.2	3.4	-5.29	-3.60	1.69	0.67	11.40	0.52	4.00 ^a	[33]
P30a	67.0	3.8	-5.62	-3.80	1.82	0.96	9.24	0.64	5.67 ^a	[68]
P30b	66.8	3.4	-5.50	-3.69	1.81	0.89	12.67	0.73	8.24 ^a	[68]
P31a	15.2	1.4	-5.51	-3.56	2.01	0.76	3.97	0.46	1.37 ^a	[69]
P31b	14.3	2.3	-5.44	-3.54	1.98	0.86	8.72	0.61	4.58 ^a	[69]
P31c	15.3	1.8	-5.40	-3.55	1.92	0.82	9.66	0.67	5.34 ^a	[69]

^a PC₆₁BM as the acceptor ^b PC₇₁BM as the acceptor

3. SUMMARY AND OUTLOOK

This paper briefly reviewed the effect of chalcogen atoms on the structural, optical, electrochemical, and photovoltaic properties of benzodichalcogenophene-based polymers. On the basis of the position of substitution, the study had divided into three sections, group 16 atoms in the donor moiety, acceptor moiety or as a spacer in the conjugated polymers. The degree of chalcogen influence varies as the substitution's position change. Compare to side chains, the effect of substitution on both optoelectronic and physical properties of polymers is more significant when it happens in the conjugated backbone.

Replacing thiophene side chains with furan slightly uplift the HOMO level which contradicts the overall substitution effect of furan in polymers. The introduction of furan is either a donor, acceptor, or π -bridge lowers the HOMO level, leading to a higher V_{OC} and better air stability. The substitution of thiophene by selenophene unit in the donor moiety, however, brings negligible effect on the energy levels and bandgap of polymers. In the case of acceptor moiety, selenium substitution concurrently increases HOMO and decreases LUMO levels of polymers, yielding a smaller bandgap and red-shifted absorption band. Depending upon the location and monomer, selenium-containing polymers can have comparable or even better photovoltaic performance than their sulfur counterparts. As for oxygen-bearing polymers, despite having higher molecular weight owing to better solubility, their performances are generally poorer than those of sulfur and selenium. The difference of thin film's morphology is a vital contributing factor.

In summary, heteroatom substitution is a promising strategy for tuning optoelectronic properties of conjugated polymers. A careful selection of appropriate substitution position is important for better performance.

ACKNOWLEDGEMENTS

Thanks for the University Malaysia Sabah for the facilities. This work was financial supported by Fundamental Research Grant Scheme under FRG0413-SG-1/2015 grant.

References

1. Y.S. Byun, J.H. Kim, J.B. Park, I.N. Kang, S.H. Jin, and D.H. Hwang, *Synth. Met.*, 168 (2013) 23.
2. H. Kim, H. Lee, Y. Jeong, J.U. Park, D. Seo, H. Heo, D. Lee, Y. Ahn, and Y. Lee, *Synth. Met.*, 211 (2016) 75.
3. M. K. Pola, K. M. Boopathi, H. Padhy, P. Raghunath, A. Singh, M.-C. Lin, C.-W. Chu, and H.-C. Lin, *Dyes Pigm.*, 139 (2017) 349.
4. P. Deng, J. Yu, X. Yin, Y. Geng, B. Zhou, F. Zhang, and W. Tang, *Dyes Pigm.*, 138 (2017) 47.
5. I. Jeong, S. Chae, A. Yi, J. Kim, H. H. Chun, J. H. Cho, H. J. Kim, and H. Suh, *Polymer*, 109 (2017) 115.
6. D. He, L. Qiu, J. Yuan, Z.-G. Zhang, Y. Li, and Y. Zou, *Polymer*, 114 (2017) 348.
7. J. Yu, X. Yin, Z. Xu, P. Deng, Y. Han, B. Zhou, and W. Tang, *Dyes Pigm.*, 136 (2017) 312.
8. J.W. Jung, J.W. Jo, E.H. Jung, and W.H. Jo, *Org. Electron.*, 31 (2016) 149.
9. H. Zhou, L. Yang, and W. You, *Macromolecules*, 45 (2012) 607.
10. B. Zhao, H. Wu, S. Liu, G. Luo, W. Wang, Z. Guo, W. Wei, C. Gao, and Z. An, *Polymer*, 116 (2017) 4.

11. Daize Mo, Huan Wang, Hui Chen, Shiwei Qu, Pengjie Chao, Zhen Yang, Leilei Tian, Yu-An Su, Yu Gao, Bing Yang, Wei Chen, and F. He, *Chem. Mater.*, 29 (2017) 2819.
12. X. Gong, S. Feng, G. Li, R. Hou, Y. Liu, Z. Zhang, C. Li, and Z. Bo, *Dyes Pigm.*, 141 (2017) 342.
13. D. He, L. Qiu, J. Yuan, Z.-G. Zhang, Y. Li, and Y. Zou, *Synth. Met.*, 226 (2017) 31.
14. D. Dang, M. Xiao, P. Zhou, J. Shi, Q. Tao, H. Tan, Y. Wang, X. Bao, Y. Liu, E. Wang, R. Yang, W. Zhu, *Org. Electron.*, 15 (2014) 2876.
15. B. Hemavathi, T.N. Ahipa, and R.K. Pai, *Eur. Polym. J.*, 72 (2015) 309.
16. Y. Li, L. Chen, Y. Chen, C. Li, P. Zhang, L. Gao, X. Yang, Y. Tu, X. Zhu, *Sol. Energ. Mat. Sol. Cells*, 108 (2013) 136.
17. H. S. Vogelbaum and G. Sauvé, *Synth. Met.*, 223 (2017) 107.
18. Y. Liang, Z. Xu, J. Xia, S.T. Tsai, Y. Wu, G. Li, C. Ray, and L. Yu, *Adv. Energ. Mater.*, 22 (2010) E135.
19. N. Allen, *Photochemistry and photophysics of polymer materials*, (2010) J. Wiley, Hoboken, New Jersey.
20. M.S. Khan, M.K. Al-Suti, J. Maharaja, A. Haque, R. Al-Balushi, and P.R. Raithby, *J. Organomet. Chem.*, 812 (2016) 13.
21. D. Gupta, S. Mukhopadhyay, and K.S. Narayan, *Sol. Energy Mater. Sol. Cells*, 94 (2010) 1309.
22. J. Yan, G. Luo, B. Xiao, H. Wu, Z. He, and Y. Cao, *Org. Electron.*, 24 (2015) 125.
23. M.S. Kim, B.G. Kim, and J. Kim, *Appl. Mater. Interfaces*, 1(6) (2009) 1264.
24. M. Jeffries-EL, B.M. Kobilka, and B.J. Hale, *Macromolecules*, 47 (21) (2014) 7253.
25. R.S. Ashraf, I. Meager, M. Nikolka, M. Kirkus, M. Planells, B.C. Schroeder, S. Holliday, M. Hurhangee, C.B. Nielsen, H. Sirringhaus, and I. McCulloch, *J. Am. Chem. Soc.*, 137 (2015) 1314.
26. M. Planells, B.C. Schroeder, and I. McCulloch, *Macromolecules*, 47(17) (2014) 5889.
27. R. Parashar and B. Negi, *Chemistry of heterocyclic compounds*, (2015) CRC, Taylor et Francis, Boca Raton, United States.
28. T. Eicher, S. Hauptmann and A. Speicher, *The Chemistry of Heterocycles*, (2012) Wiley vch, Weinheim.
29. J. Joule and K. Mills, *Heterocyclic Chemistry*, (2013) Wiley, Somerset.
30. M.E. Cinar, and T. Ozturk, *Chem. Rev.*, 115 (2015) 3036.
31. T. Krygowski and M. Cyranski, *Aromaticity in Heterocyclic Compounds*, (2009) Springer Berlin Heidelberg, Berlin, Heidelberg.
32. J. Hou, M. Park, S. Zhang, Y. Yao, L. Chen, J. Li, and Y. Yang, *Macromolecules*, 41 (2008) 6012.
33. J. Jiang, P. Raghunath, H. Lin, Y. Lin, M.C Lin, and K. Wei, *Macromolecules*, 47 (2014) 7070.
34. J. Yu, X. Yin, Z. Xu, P. Deng, Y. Han, B. Zhou, W. Tang, *Dyes Pigm.*, 136 (2017) 312.
35. L. Huo, Y. Huang, B. Fan, X. Guo, Y. Jing, M. Zhang, Y. Li, and J. Hou, *Chem. Commun.*, 48 (2012) 3318.
36. J. Hou, H. Chen, S. Zhang, and Y. Yang, *J. Phys. Chem.*, 113(50) (2009) 21202.
37. L. Xiao, B. Liu, X. Chen, Y. Li, W. Tang, and Y. Zou, *RSC Adv.*, 3 (2013) 11869.
38. S. Zhang, L. Ye, and J. Hou, *Adv. Energy Mater.*, 6(11) (2016) 1502529.
39. Z. He, C. Zhong, S. Su, M. Xu, H. Wu, and Y. Cao, *Nat. Photonics*, 6 (2012) 591.
40. B. Liu, X. Chen, Y. Zou, Y. He, L. Xiao, X. Xu, L. Li, and Y. Li, *Polym. Chem.*, 4 (2013) 470.
41. L. Huo, L. Ye, Y. Wu, Z. Li, X. Guo, M. Zhang, S. Zhang, and J. Hou, *Macromolecules*, 45 (2012) 6923.
42. H. Cheng, J. Hou, S. Zhang, Y. Liang, G. Yang, Y. Yang, L. Yu, Y. Wu, and G. Li, *Nat. Photonics*, 3 (2009) 649.
43. L. Huo, Z. Li, X. Guo, Y. Wu, M. Zhang, L. Ye, S. Zhang, and J. Hou, *Polym. Chem.*, 4 (2013) 3047.
44. Y. Liang, D. Feng, Y. Wu, S. Tsai, G. Li, C. Ray, and L. Yu, *J. Am. Chem. Soc.*, 131(22) (2009) 7792.

45. H.A. Saedah, L. Lu, F. He, J.E. Bullock, W. Wang, B. Carsten, and L. Yu, *ACS Macro Lett.*, 1 (2012) 361.
46. C. Liu, C. Yi, K. Wang, Y. Yang, R. S. Bhatta, M. Tsige, S. Xiao, and X. Gong, *ACS Appl. Mater. Interfaces*, 7(8) (2015) 4928.
47. Z. Cong, B. Zhao, H. Wu, Z. Guo, W. Wang, G. Luo, J. Xu, Y. Xia, C. Gao, and Z. An, *Polym.*, 67 (2015) 55.
48. H. Wu, B. Zhao, W. Wang, Z. Guo, W. Wei, Z. An, G. Chao, H. Chen, B. Xiao, Y. Xie, H. Wu, Y. Cao, *J. Mater. Chem. A*, 3 (2015) 18115.
49. M. Tessarolo, D. Gedefaw, M. Bolognesi, F. Liscio, P. Henriksson, W. Zhuang, S. Milita, M. Muccini, E. Wang, M. Seri, and M.R. Andersson, *J. Mater. Chem. A*, 2 (2014) 11162.
50. Y. Zhang, L. Gao, C. He, Q. Sun, and Y. Li, *Polym. Chem.*, 4 (2013) 1474.
51. Y. Wang, Y. Liu, S. Chen, R. Peng, and Z. Ge, *Chem. Mater.*, 25 (2013) 3196.
52. J. Jiang, H. Lin, Y. Lin, H. Chen, S. Lan, C. Chang, and K. Wei, *Macromolecules*, 47 (2014) 70.
53. S. Zhang, L. Ye, W. Zhao, D. Liu, H. Yao, and J. Hou, *Macromolecules*, 47 (2014) 4653.
54. P. Huang, J. Du, S.S. Gunathilake, E.A. Rainbolt, J.W. Murphy, K.T. Black, D. Barrera, J.W.P. Hsu, B.E. Gnade, M.C. Stefan, and M.C. Biewer, *J. Mater. Chem. A*, 3 (2015) 6980.
55. J. Warnan, A.E. Labban, C. Cabanetos, E.T. Hoke, P.K. Shukla, C. Risko, J. Brédas, M.D. McGehee, and P.M. Beaujuge, *Chem. Mater.*, 26 (2014) 2299.
56. N. Chakravarthi, K. Kranthiraja, K. Gunasekar, Y.-S. Gal, Y.-R. Cho, and S.-H. Jin, *Synth. Met.*, 222 (2016) 2.
57. J. Yuan, X. Huang, F. Zhang, J. Lu, Z. Zhai, C. Di, Z. Jiang, and W. Ma, *J. Mater. Chem.*, 22 (2012) 22734.
58. Y. Wang, F. Yang, Y. Liu, R. Peng, S. Chen, Z. Ge, *Macromolecules*, 46 (2013) 1368.
59. K. Wang, W. Su, X. Guo, M. Zhang, and Y. Li, *Org. Electron.*, 33 (2016) 15.
60. K. Kranthiraja, K. Gunasekar, W. Cho, Y.G. Park, J.Y. Lee, Y. Shin, I. Kang, M. Song, K.H. Chae, B. Kim, and S. Jin, *J. Mater. Chem. C*, 3 (2015) 796.
61. L. Dou, W. Chang, J. Gao, C. Chen, J. You, Y. Yang, *Adv. Mater.*, 25 (2013) 825.
62. V. Tamilavan, K.H. Roh, R. Agneeswari, D.Y. Lee, S. Cho, Y. Jin, S.H. Park, and M.H. Hyun, *J. Polym. Sci.*, 52 (2014) 3564.
63. V. Tamilavan, J.B. Park, I. Kang, D. Hwang, and M.H. Hyun, *Synth. Met.*, 198 (2014) 230.
64. B. Liu, X. Chen, Y. Zou, L. Xiao, X. Xu, Y. He, L. Li, and Y. Li, *Macromolecules*, 45 (2012) 6898.
65. E. Zhou, J. Cong, K. Hashimoto, and K. Tajima, *Macromolecules*, 46 (2013) 763.
66. B. Liu, X. Chen, Y. He, Y. Li, X. Xu, L. Xiao, L. Li, and Y. Zou, *J. Mater. Chem. A*, 1 (2013) 570.
67. S.A. Shin, J.B. Park, J. Kim, and D. Hwang, *Synth. Met.*, 172 (2013) 54.
68. G. Li, X. Gong, J. Zhang, Y. Liu, S. Feng, C. Li, and Z. Bo, *Appl. Mater. Interfaces*, 8 (2016) 3686.
69. J. Lee, D. H. Sin, J. A. Clement, C. Kulshreshtha, H. G. Kim, E. Song, J. Shin, H. Hwang, and K. Cho, *Macromolecules*, 49(24) (2016) 9358.
70. A. Efrem, Y. Lei, B. Wu, M. Wang, S. C. Ng, and B. S. Ong, *Dyes Pigm.*, 129 (2016) 90.